IEEE Access
Multidisciplinary | Rapid Review | Open Access Journal

Received 27 August 2022, accepted 10 September 2022, date of publication 19 September 2022, date of current version 5 October 2022.

Digital Object Identifier 10.1109/ACCESS.2022.3207783

RESEARCH ARTICLE

Three-Phase Power Flow Calculations Using Initial Voltage Estimation Method for Unbalanced Distribution Networks

NIEN-CHE YANG, (Member, IEEE), MENG-JIA LIU, KAI-YOU LAI, AND EUNIKE WIDYA ADINDA

Department of Electrical Engineering, National Taiwan University of Science and Technology, Taipei 10607, Taiwan

Corresponding author: Nien-Che Yang (ncyang@mail.ntust.edu.tw)

This work was supported in part by the Ministry of Science and Technology (MOST) in Taiwan, in part by MOST under Grant MOST 110-2622-8-011-012-SB, and in part by the Delta Electronics (DELTA)—National Taiwan University of Science of Technology (NTUST) Joint Research Center.

ABSTRACT In this study, we propose a three-phase power-flow calculation using the initial voltage estimation for unbalanced radial distribution systems. Graph theory, Kron reduction, and injection current methods are combined in the proposed method. Network components, such as transmission lines, transformers, and loads, are integrated into the system bus impedance matrix ($\mathbf{Z}_{BUS}$). If there are only network components with constant or quasi-constant impedance characteristics in distribution systems, the power flow can be solved without iterative procedures. Therefore, the proposed method can be called the ''direct solution method''. Because the initial estimations can approximate the final converged solutions, the proposed method has excellent convergence capability. To demonstrate the feasibility and effectiveness of the proposed method, five IEEE test systems are used for comparisons in different scenarios. The test results demonstrate that the proposed method performs well by offering good convergence in complex distribution networks with different transformer connections.

INDEX TERMS Distribution network, distribution transformer modeling, power flow analysis, three-phase power flow, unbalanced power network.

I. INTRODUCTION

In recent years, due to the rapid economic development of countries, people's standards of living have continued to improve. The industrial and commercial sectors are booming, and electricity consumption continues to increase annually. With the increase in green energy awareness, many renewable energy sources have been added to power grids. Research on transmission and distribution systems has expanded. The planning, design, operation, and maintenance of distribution systems and the quality and reliability of the power supply must be evaluated using a complete and accurate power flow analysis tool. Therefore, developing a powerful three-phase power-flow analysis method is necessary to address the complexity and variety of distribution systems.

The purpose of the power flow study is to determine the electrical quantities of the entire power system under the given operating conditions and network topologies. In other words, the bus voltage magnitudes and angles, line power flows, and line power losses can be determined. The results of power flow calculations are the basis for stability and fault studies. The development of these methods is based on some basic requirements, which can be summarized as follows:

1. Reliability and convergence of algorithms;
2. Calculation speed and memory usage;
3. Convenience and flexibility of calculations.

Research on power flow analysis began in 1956 and has been ongoing since then. Various calculation methods for power flow studies, including Gauss-Seidel and

The associate editor coordinating the review of this manuscript and approving it for publication was Zhouyang Ren.

Newton-Raphson (NR) methods [1], [2], have been developed. However, they are generally only applicable to transmission networks and are not significantly compatible with low-voltage distribution networks. Most distribution systems operate in a radial arrangement, i.e., when power flow is unidirectional. The distribution network supplies electricity directly to the end customers with lower voltage levels and smaller transmission capacities. The cross-sectional area of the conductors is smaller, resulting in a large R/X ratio of the feeders. Therefore, the traditional power flow calculation for transmission networks cannot be directly applied to power flow calculations for distribution networks.

Several algorithms have been designed for distribution networks with radial arrangements. From the viewpoint of network analysis, algorithms can be divided into two main categories: nodal voltage and branch current analyses. Typical nodal voltage analysis methods include modified NR and fast decoupling [3]. The improved NR method conforms to the topological characteristics of distribution networks. However, the NR method is significantly influenced by the initial guess of the iterative process, which must be close to the final converged results. Otherwise, the iteration diverges easily.

Owing to the large R/X of the distribution networks, the boundary conditions of the fast decoupling method cannot be satisfied. Thus, it is difficult to obtain the desired converged results when calculating the power flows of the distribution networks. Nevertheless, some studies have been conducted to improve the fast decoupling method applicable to distribution networks [4], [5], [6]. The modified fast decoupling methods may lose the original small computation and reliable convergence features by improving the $\boldsymbol{B}^{'}$ and $\boldsymbol{B}^{''}$ matrices to handle line conductors with large R/X.

Branch-current analysis method is the most popular algorithm for distribution power-flow calculations. These types of solution algorithms can be categorized as follows: the loop-impedance method [7], forward/backward sweep [8], [9], [10], [11], ladder, and direct $\mathbf{Z}_{BUS}$ methods [12]. These type of algorithms exhibit the characteristics of a simple algorithm and reliable convergence. In the loop-impedance method, the load at the node is represented by a constant impedance without considering line-to-ground conductances in the distribution networks, and the number of branches in the distribution networks is larger than the number of links. Therefore, the loop-current method is suitable for power-flow studies. From the slack bus to each load node, it forms a loop. A distribution network consists of a finite number of loops. The bus voltage can be determined using Kirchhoff's law of voltage.

In recent years, the forward/backward sweep method has been widely used in power flow studies of distribution networks. According to the breadth priority, all branch components are numbered hierarchically for the sequence of iteration steps. Moreover, this type of method, with simple and practical characteristics, does not require the formation of a conductance or impedance matrix. In the second method, the line power loss is regarded as the state quantity. The effects of the reactive powers and line voltage drops on the line power losses are considered. In the forward sweep process, the node voltages are obtained from the injected powers at the nodes. The line power losses are updated in the backward sweep process using new node voltages. The new node voltages are then iteratively updated by the nodal injected powers until convergence is achieved.

In the direct $\mathbf{Z}_{BUS}$ method, graph theory is used to build a constant bus impedance matrix with series impedances for the branch components. During the iterative process, the shunt conductances of the feeder conductors, mutual couplings of the transformers, and load demands are represented as equivalent injected currents. Convergence is achieved when the difference between the bus voltages obtained by two successive iterations is less than the preset tolerance.

The aforementioned power flow solution algorithms require an iteration process. Therefore, the holomorphic embedding load flow method (HELM) was used to solve this problem [13], [14] based on complex analysis. The HELM embeds the original physical power flow problem into the holomorphic function for mapping the corresponding voltages, ensuring the definiteness of the final solution. The HELM is non-iterative and deterministic. However, the accuracy requirement and computation effort of HELM are still in concern. The accuracy of the computation process must be improved by combining iteration processes [15].

Finally, the purpose of this study is to develop a methodology to improve the solution procedure of the direct $\mathbf{Z}_{BUS}$ method. In the proposed method, both the series and shunt impedances are involved in the bus impedance matrix. The initial estimations approximate the final converged solutions. The convergence solution can be quickly obtained using negligible compensation currents. The results demonstrate that the proposed method exhibits excellent convergence, robustness, and feasibility.

II. DISTRIBUTION SYSTEM COMPONENT MODELS

Theoretically, distribution systems are more complex than transmission systems because of various network components and load demand behaviors. Additionally, the topology of distribution systems is inherently asymmetrical. Network component models may affect the accuracy and convergence of solution algorithms. The selection of the network component models corresponds to the solution algorithms. However, a trade-off between the accuracy of the network component models and the convergence of the solution algorithms is a challenge.

Network components in power systems can be divided into series and shunt components. In general, series and shunt components are represented as resistances, inductances and capacitances, or injected currents. In the direct $\mathbf{Z}_{BUS}$ method, the resistances, inductances and capacitances were integrated into the bus impedance matrix. The shunt components were represented as injected currents. In the proposed method, the phase-to-ground shunt component is equivalent to

a constant-impedance and injection-current source. Therefore, when building the bus impedance matrix, the series components of the distribution networks are first involved, and then the shunt components are considered using the Kron reduction method.

A. TRANSMISSION LINE MODEL

In this study, the transmission lines are represented as π model equivalent circuits [16], [17], [18], [19], as shown in Fig. 1. Using the Carson equation, the self-impedance and phase-to-phase mutual impedance of each phase as well as the shunt self-inductance and mutual inductance can be calculated. Moreover, the series impedance matrix and shunt capacitance matrix with the implied neutral or ground wire effect can be obtained using the Kron reduction, as shown in (1) and (2). The charging capacitances between conductors or between conductor and ground are represented as shunt capacitances, as shown in Fig. 2 (a), and the charging capacitances are expressed as equivalent impedances, as shown in Fig. 2 (b).

$$[z^{abc}]_{line} = \begin{bmatrix} z^{aa-g} & z^{ab-g} & z^{ac-g} \\ z^{ba-g} & z^{bb-g} & z^{bc-g} \\ z^{ca-g} & z^{cb-g} & z^{cc-g} \end{bmatrix} \Omega/\text{mile} \quad (1)$$

$$[C^{abc}]_{line} = \begin{bmatrix} C^{aa-g} & C^{ab-g} & C^{ac-g} \\ C^{ba-g} & C^{bb-g} & C^{bc-g} \\ C^{ca-g} & C^{cb-g} & C^{cc-g} \end{bmatrix} \mu F/\text{mile} \quad (2)$$

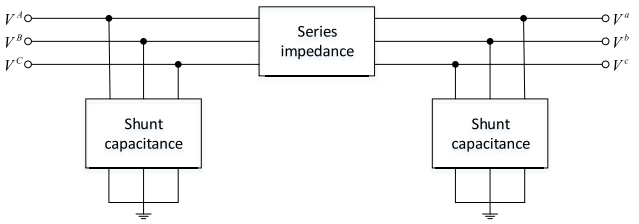

FIGURE 1. Transmission line π-equivalent model.

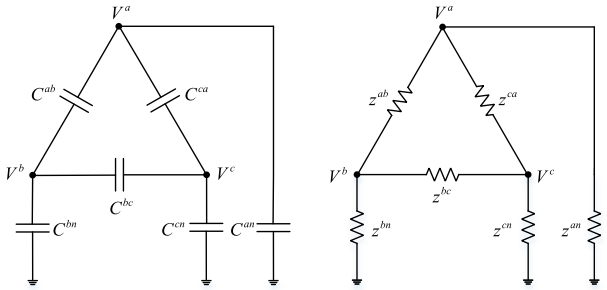

(a) Charging capacitance equivalent model (b) Charging capacitance equivalent impedance Model

FIGURE 2. Equivalent model of charging capacitance and equivalent impedance of three-phase conductor.

By integrating the series impedance model and shunt impedance equivalent model, the complete equivalent model for the three-phase three-wire transmission line used in the proposed algorithm can be obtained, as shown in Fig. 3.

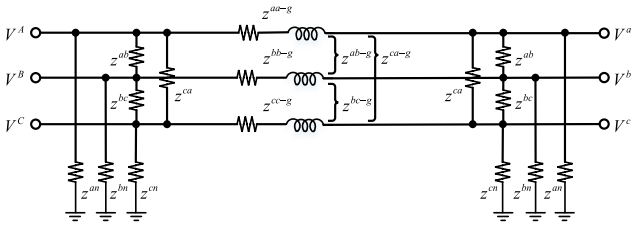

FIGURE 3. Three-phase three-wire transmission line equivalent model.

B. TRANSFORMER MODEL

In this study, an equivalent model for three-phase three-wire distribution transformers [19], [20] is used for the proposed algorithm using single-phase two-wire transformer models and the superposition method. Here, the $Y_g - Y_g$ transformer is used as an example. The primary and secondary winding taps of the transformers are α and β, respectively, and the bus admittance matrix for the distribution transformers is shown in (3).

$$[Y^{abc}]_{tr} = \begin{bmatrix} \frac{y_t}{\alpha^2} & & & -\frac{y_t}{\alpha\beta} & & \\ & \frac{y_t}{\alpha^2} & & & -\frac{y_t}{\alpha\beta} & \\ & & \frac{y_t}{\alpha^2} & & & -\frac{y_t}{\alpha\beta} \\ -\frac{y_t}{\alpha\beta} & & & \frac{y_t}{\beta^2} & & \\ & -\frac{y_t}{\alpha\beta} & & & \frac{y_t}{\beta^2} & \\ & & -\frac{y_t}{\alpha\beta} & & & \frac{y_t}{\beta^2} \end{bmatrix} \quad (3)$$

where y_t is the per-unit (p.u.) leakage admittance measured using the short-circuit test.

The decoupled circuit can be determined using the bus admittance matrix. Only the self-admittances in the decoupled circuit are retained and expressed in terms of the impedance, as shown in (4). The mutual inductances are expressed as the equivalent shunt impedances, as shown in Fig. 4.

$$[z_{prim}]_{tr} = \begin{bmatrix} \frac{\alpha\beta}{y_t} & 0 & 0 \\ 0 & \frac{\alpha\beta}{y_t} & 0 \\ 0 & 0 & \frac{\alpha\beta}{y_t} \end{bmatrix} \quad (4)$$

C. LOAD MODEL

The loads can be divided into a lumped load connected to the nodes and a load evenly distributed along the feeder. Depending on the number of phases, loads can be divided into three- and single-phase load demands. Three-phase loads can be connected as Y-connected or Δ-connected loads, whereas single-phase loads can be connected between the

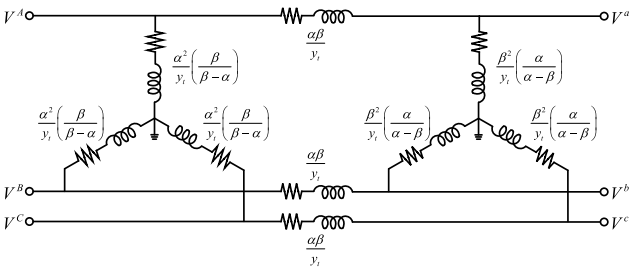

FIGURE 4. Equivalent impedance model for $Y_g - Y_g$ transformer.

phase and neutral wires or between the phase and phase wires. Depending on the load behavior, the loads can be classified as constant impedance (Z), constant current (I), or constant power (P) loads [19], [21]. In this study, a ZIP load model was adopted, as shown in Fig. 5.

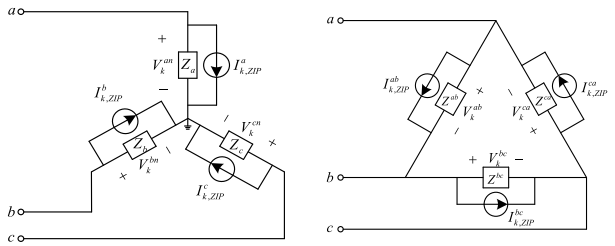

(a) Y-connection load (b) Δ-connection load

FIGURE 5. ZIP load model.

However, the load power depends on the phase voltage and load behavior. Therefore, the load power $S^i_{k,ZIP}$ for each phase connected to bus-k is calculated, as shown in (5).

$$S^i_{k,ZIP} = S^i_{0,ZIP}\left[a_0 + a_1 \cdot \left[\frac{V^i_k}{V^i_0}\right]^1 + a_2 \cdot \left[\frac{V^i_k}{V^i_0}\right]^2\right], \quad i \in \{a, b, c\} \tag{5}$$

where $S^i_{k,ZIP}$ are the load complex powers with operating phase voltages V^i_k and $S^i_{0,ZIP}$ is the load complex power at the rated phase voltage V^i_0. In addition, a_0, a_1, and a_2 are the load coefficients for constant power, current, and impedance loads, respectively. Here, $a_0 + a_1 + a_2 = 1$.

In this study, the load powers were decomposed into two parts: (1) the rated load impedance Z^i and (2) the compensation injection current I^i_k. The rated load impedance is determined by the rated power and rated phase voltage. The load impedance Z^i is calculated for each phase using (6).

$$Z^i = \frac{|V^i_0|^2}{S^i_0}, \quad i \in \{a, b, c\} \tag{6}$$

where V^i_0 is the rated phase voltage and S^i_0 is the rated complex power.

Furthermore, the constant Z load complex power S^i_z at phase voltage V^i_k is shown in (7). The mismatch between the ZIP load complex power $S^i_{k,ZIP}$ and the constant Z-load complex power S^i_z are corrected using injection current compensation. The compensating injection current $I^i_{k,ZIP}$ for each phase at bus k is calculated using (8).

$$S^i_z = V^i_k \cdot \left(\frac{V^i_k}{Z_i}\right)^*, \quad i \in \{a, b, c\} \tag{7}$$

$$I^i_{k,ZIP} = -\left(\frac{S^i_{k,ZIP} - S^i_z}{V^i_k}\right)^*, \quad i \in \{a, b, c\} \tag{8}$$

III. NETWORK PERFORMANCE EQUATIONS

A. GRAPH THEORY

In 1736, Swiss mathematician Euler solved the seven-bridge problem. Thus, graph theory was initiated. Graph theory focuses on collecting nodes and edges to graphically describe the geometric relationships of their network topologies. As computing speed increases, electrical system analysis techniques have also changed considerably. Since then, scholars have introduced graph theory into electrical power system studies. A complex network topology is regarded as a geometric graph of nodes and line segments. The connection relationship of the electrical system components is described by the corresponding incidence matrix [22].

To facilitate the derivation of the incidence matrix, a single-line diagram of a simple radial distribution system was used, as shown in Fig. 6. In traditional power system studies, a slack bus is often considered to be the ideal voltage source. However, the internal impedance of the slack bus was considered in the proposed algorithm. The single-line diagram shown in Fig. 6 has been modified, as shown in Fig. 7.

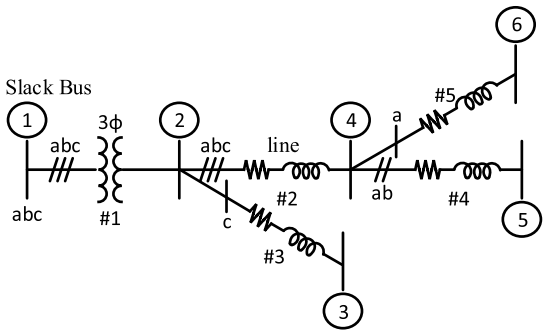

FIGURE 6. Single-line diagram for radial power distribution system.

In a radial power system with n nodes, the e elements and b branches can be determined using $b = e = n - 1$. In Fig. 7, the $n = 7$, therefore $e = 6$ and $b = 6$. Additionally, the following section introduces the incidence matrices used in this study, consisting of an element-node incidence matrix $\hat{\mathbf{E}}$, bus incidence matrix $\mathbf{E}$, and branch-path incidence matrix $\mathbf{B}$.

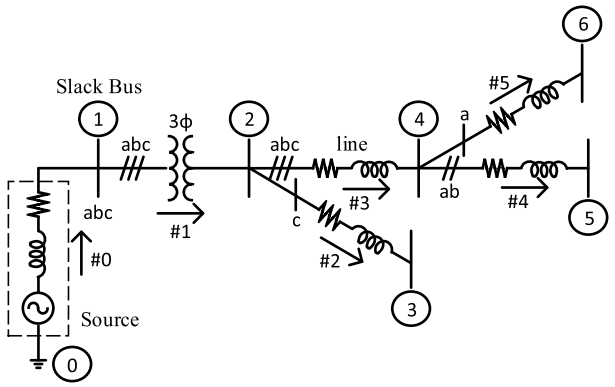

FIGURE 7. Single-line diagram with a voltage source model.

1) ELEMENT-NODE INCIDENCE MATRIX $\hat{\mathbf{E}}$

The element-node incidence matrix $\hat{\mathbf{E}}$ is defined as a matrix with $e \times n$ dimensions, describing the connection relationship of a power grid mainly through the association of elements and nodes, which is described as follows:

$\hat{\mathbf{E}}(i,j) = +\mathbf{U}$: The i-th element is connected to the j-th node and is oriented to outflow the j-node.

$\hat{\mathbf{E}}(i,j) = -\mathbf{U}$: The i-th element is connected to the j-th node and is oriented to flow into the j-th node.

$\hat{\mathbf{E}}(i,j) = 0$: The i-th element has no connection to the j-th node.

where $\mathbf{U}$ is the unit matrix. For single-phase, two-phase, and three-phase elements, the dimensions were 1×1, 2×2, and 3×3, respectively, and the remaining unconnected elements were zero matrices. In Fig. 7, the element-node incidence matrix $\hat{\mathbf{E}}$ is expressed as follows:

$$\hat{\mathbf{E}} = \begin{array}{c} \\ a \\ \#0\,b \\ c \\ a \\ \#1\,b \\ c \\ \hat{\mathbf{E}}=\#2\,c \\ a \\ \#3\,b \\ c \\ a \\ \#4\,b \\ \#5\,a \end{array} \begin{array}{c} \begin{array}{cccccccccccccccccc} \textcircled{0} & & & \textcircled{1} & & & \textcircled{2} & & & \textcircled{3} & \textcircled{4} & & & \textcircled{5} & & \textcircled{6} \\ a & b & c & a & b & c & a & b & c & c & a & b & c & a & b & a \end{array} \\ \begin{bmatrix} 1 & & & -1 & & & & & & & & & & & & \\ & 1 & & & -1 & & & & & & & & & & & \\ & & 1 & & & -1 & & & & & & & & & & \\ \hline & & & 1 & & & -1 & & & & & & & & & \\ & & & & 1 & & & -1 & & & & & & & & \\ & & & & & 1 & & & -1 & & & & & & & \\ \hline & & & & & & & & 1 & -1 & & & & & & \\ \hline & & & & & & 1 & & & & -1 & & & & & \\ & & & & & & & 1 & & & & -1 & & & & \\ & & & & & & & & 1 & & & & -1 & & & \\ \hline & & & & & & & & & & 1 & & & -1 & & \\ & & & & & & & & & & & 1 & & & -1 & \\ \hline & & & & & & & & & & & & & & & -1 \end{bmatrix} \end{array} \tag{9}$$

2) BUS INCIDENCE MATRIX $\mathbf{E}$

The bus incidence matrix $\mathbf{E}$ is defined as a matrix with $e \times (n-1)$ dimensions, where the element-node incidence matrix $\hat{\mathbf{E}}$ is obtained by deleting the corresponding column of the reference node. Any node can be selected as a reference. The ground node ⓪ at the system voltage source was selected as a reference in the proposed algorithm. The bus incidence matrix $\mathbf{E}$ for Fig. 7 is expressed as follows:

$$\mathbf{E} = \begin{array}{c} \\ a \\ \#0\,b \\ c \\ a \\ \#1\,b \\ c \\ \mathbf{E}=\#2\,c \\ a \\ \#3\,b \\ c \\ a \\ \#4\,b \\ \#5\,a \end{array} \begin{array}{c} \begin{array}{cccccccccccccccccc} \textcircled{1} & & & \textcircled{2} & & & \textcircled{3} & & & \textcircled{4} & & & \textcircled{5} & & \textcircled{6} \\ a & b & c & a & b & c & c & a & b & c & a & b & a \end{array} \\ \begin{bmatrix} -1 & & & & & & & & & & & & & \\ & -1 & & & & & & & & & & & & \\ & & -1 & & & & & & & & & & & \\ \hline 1 & & & -1 & & & & & & & & & & \\ & 1 & & & -1 & & & & & & & & & \\ & & 1 & & & -1 & & & & & & & & \\ \hline & & & & & & 1 & -1 & & & & & & \\ \hline & & & 1 & & & & & -1 & & & & & \\ & & & & 1 & & & & & -1 & & & & \\ & & & & & 1 & & & & & -1 & & & \\ \hline & & & & & & & 1 & & & & -1 & & \\ & & & & & & & & 1 & & & & -1 & \\ \hline & & & & & & & & & & 1 & & & -1 \end{bmatrix} \end{array} \tag{10}$$

3) BRANCH-PATH INCIDENCE MATRIX $\mathbf{B}$

The branch-path incidence matrix $\mathbf{B}$ is defined as a matrix with $e \times (n-1)$ dimensions, expressing the relationship between the branches and paths. Path refers to the branches from the corresponding bus to the reference. The branch path incidence matrix $\mathbf{B}$ is described as follows:

$\mathbf{B}(i,j) = +\mathbf{U}$: The i-th branch is from the j-th node to the reference and is oriented in the same direction.

$\mathbf{B}(i,j) = -\mathbf{U}$: The i-th branch path is from the j-th node to the reference and is oriented in the opposite direction.

$\mathbf{B}(i,j) = 0$: The i-th branch has no connection to the j-th node.

In Fig. 7, the branch-path incidence matrix $\mathbf{B}$ is expressed as follows:

$$\mathbf{B} = \begin{array}{c} \\ a \\ \#0\,b \\ c \\ a \\ \#1\,b \\ c \\ \mathbf{B}=\#2\,c \\ a \\ \#3\,b \\ c \\ a \\ \#4\,b \\ \#5\,a \end{array} \begin{array}{c} \begin{array}{cccccccccccccccccc} \textcircled{1} & & & \textcircled{2} & & & \textcircled{3} & & & \textcircled{4} & & & \textcircled{5} & & \textcircled{6} \\ a & b & c & a & b & c & c & a & b & c & a & b & a \end{array} \\ \begin{bmatrix} -1 & & & -1 & & & & -1 & & & -1 & & -1 \\ & -1 & & & -1 & & & & -1 & & & -1 & \\ & & -1 & & & -1 & -1 & & & -1 & & & \\ \hline & & & -1 & & & & -1 & & & -1 & & -1 \\ & & & & -1 & & & & -1 & & & -1 & \\ & & & & & -1 & -1 & & & -1 & & & \\ \hline & & & & & & -1 & & & & & & \\ \hline & & & & & & & -1 & & & -1 & & -1 \\ & & & & & & & & -1 & & & -1 & \\ & & & & & & & & & -1 & & & \\ \hline & & & & & & & & & & -1 & & \\ & & & & & & & & & & & -1 & \\ \hline & & & & & & & & & & & & -1 \end{bmatrix} \end{array} \tag{11}$$

Because the power grid is a radial arrangement with no link circuit, the bus incidence matrix has the following relationship with the branch-path incidence matrix.

$$\mathbf{E}^t\mathbf{B} = \mathbf{U} \tag{12}$$

$$\mathbf{B} = (\mathbf{E}^t)^{-1} \tag{13}$$

However, network component models describe the connection relationship of the network components and the characteristics of the individual network components.

B. SERIES COMPONEN BUILDING ALGORITHM

According to the graph theory mentioned in the previous section, network components were divided into series and shunt components. The set of series components does not constitute a loop, whereas any shunt component can be added to constitute a loop.

Each component in a network can be expressed in impedance or admittance form. The characteristics of the network components can be represented as the primitive impedance matrix $\mathbf{z}^{a,b,c}$ or primitive admittance matrix $\mathbf{y}^{a,b,c}$, as shown in Fig. 8.

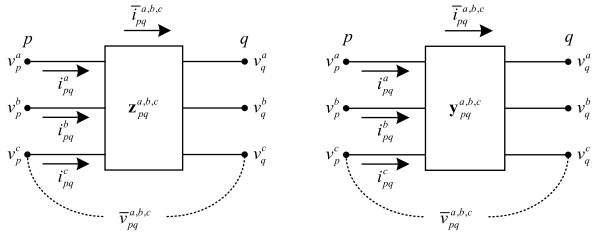

(a) Impedance form (b) Admittance form

FIGURE 8. Representations of a network component.

Therefore, the performance equations of a primitive network in impedance form and admittance form can be expressed as

$$\bar{v}^{a,b,c} = \left[z^{a,b,c}\right] \cdot \bar{i}^{a,b,c} \tag{14}$$

$$\bar{i}^{a,b,c} = \left[y^{a,b,c}\right] \cdot \bar{v}^{a,b,c} \tag{15}$$

is multiplied by the transpose matrix of the bus incidence matrix $\mathbf{E}^t$. According to Kirchhoff's current law, the current injected into the bus yields

$$\bar{I}_{BUS}^{a,b,c} = \mathbf{E}^t \bar{i}^{a,b,c} = \mathbf{E}^t \left[y^{a,b,c}\right] \cdot \bar{v}^{a,b,c} \tag{16}$$

According to the conservation of energy law, the power in interconnected and primitive networks must be equal, i.e.,

$$\left(\bar{I}_{BUS}^{*a,b,c}\right)^t \bar{V}_{BUS}^{a,b,c} = \left(\bar{i}^{*a,b,c}\right)^t \bar{v}^{a,b,c} \tag{17}$$

Then, by substituting (16) into (17), yields

$$\left(\bar{i}^{*a,b,c}\right)^t \mathbf{E} \bar{V}_{BUS}^{a,b,c} = \left(\bar{i}^{*a,b,c}\right)^t \bar{v}^{a,b,c} \tag{18}$$

Therefore,

$$\bar{v}^{a,b,c} = \mathbf{E} \bar{V}_{BUS}^{a,b,c} \tag{19}$$

Substituting (19) into (16), yields

$$\bar{I}_{BUS}^{a,b,c} = \mathbf{E}^t \left[y^{a,b,c}\right] \mathbf{E} \bar{V}_{BUS}^{a,b,c} \tag{20}$$

Therefore, using the bus frame of reference, the performance equation of a network in the admittance form is expressed as follows:

$$\bar{I}_{BUS}^{a,b,c} = \mathbf{Y}_{BUS}^{a,b,c} \bar{V}_{BUS}^{a,b,c} \tag{21}$$

According to (21), it can be seen that the bus admittance matrix $\mathbf{Y}_{BUS}^{a,b,c}$ is obtained by multiplying the bus incidence matrix $\mathbf{E}$ with the primitive series admittance matrix $\left[y^{a,b,c}\right]$. The bus impedance matrix $\mathbf{Z}_{BUS}^{a,b,c}$ is the inverse of the bus admittance matrix $\mathbf{Y}_{BUS}^{a,b,c}$, as expressed in (22).

$$\mathbf{Z}_{BUS}^{a,b,c} = \left(\mathbf{Y}_{BUS}^{a,b,c}\right)^{-1} = \left(\mathbf{E}^t \left[y^{a,b,c}\right] \mathbf{E}\right)^{-1} \tag{22}$$

According to the relationship between the bus incidence matrix $\mathbf{E}$ and branch-path incidence matrix $\mathbf{B}$, yields

$$\mathbf{Z}_{BUS}^{a,b,c} \equiv \mathbf{B}^t \left[z^{a,b,c}\right] \mathbf{B} \tag{23}$$

C. SHUNT COMPONENT BUILDING ALGORITHM

According to (23), the topology of distribution networks can be described by the corresponding incidence matrix. The dimension of the $\mathbf{Z}_{BUS}$ is unchanged when an element (link) is added between the existing nodes. All elements of the original bus impedance matrix must be recalculated to include the effect of the added link by using the Kron reduction method [23], [24].

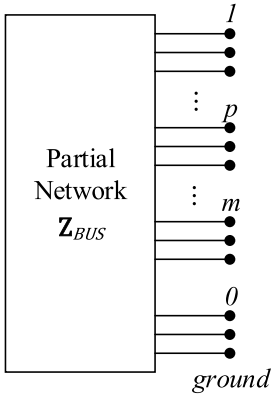

FIGURE 9. Representation of a partial network.

We assume a partial network with m buses and reference node 0, as shown in Fig. 9. $\mathbf{Z}_{BUS}$ is the series impedance matrix of the partial network. The performance equation of the partial network can be expressed in (24).

$$\begin{aligned}
\bar{V}_1^{a,b,c} &= \mathbf{Z}_{11}^{a,b,c}\bar{I}_1^{a,b,c} + \ldots + \mathbf{Z}_{1p}^{a,b,c}\bar{I}_p^{a,b,c} + \ldots \\
&\quad + \mathbf{Z}_{1m}^{a,b,c}\bar{I}_m^{a,b,c} \\
&\vdots \\
\bar{V}_p^{a,b,c} &= \mathbf{Z}_{p1}^{a,b,c}\bar{I}_1^{a,b,c} + \ldots + \mathbf{Z}_{pp}^{a,b,c}\bar{I}_p^{a,b,c} + \ldots \\
&\quad + \mathbf{Z}_{pm}^{a,b,c}\bar{I}_m^{a,b,c} \\
&\vdots \\
\bar{V}_m^{a,b,c} &= \mathbf{Z}_{m1}^{a,b,c}\bar{I}_1^{a,b,c} + \ldots + \mathbf{Z}_{mp}^{a,b,c}\bar{I}_p^{a,b,c} + \ldots \\
&\quad + \mathbf{Z}_{mm}^{a,b,c}\bar{I}_m^{a,b,c}
\end{aligned} \tag{24}$$

When a link is added to the partial network between bus p and bus q, no new buses are added. The dimensions of the

$\mathbf{Z}_{BUS}$ matrix remain unchanged, but all elements in $\mathbf{Z}_{BUS}$ matrix must be recalculated. If the impedance of the added link is $\mathbf{z}_{pq}^{a,b,c}$ and there is a current $\bar{I}_l^{a,b,c}$ flowing through this impedance, as shown in Fig. 10 (a). Therefore, from Fig. 10 (a), we obtain

$$\bar{V}_q^{a,b,c} - \bar{V}_p^{a,b,c} + \mathbf{z}_{pq}^{a,b,c}\bar{I}_l^{a,b,c} = 0 \tag{25}$$

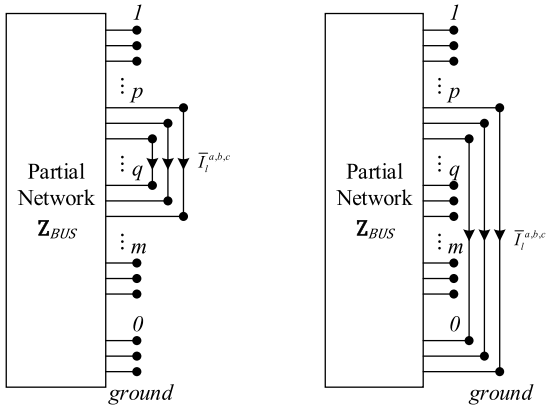

(a) A link between two existing buses

(b) A link between a bus and the ground

FIGURE 10. Add a link.

By adding a link, the original currents $\bar{I}_p^{a,b,c}$ and $\bar{I}_q^{a,b,c}$ were changed to $\bar{I}_p^{a,b,c} - \bar{I}_l^{a,b,c}$ and $\bar{I}_q^{a,b,c} + \bar{I}_l^{a,b,c}$, respectively. Therefore, the network equation becomes:

$$\begin{aligned}
\bar{V}_1^{a,b,c} &= \mathbf{Z}_{11}^{a,b,c}\bar{I}_1^{a,b,c} + \ldots + \mathbf{Z}_{1p}^{a,b,c}\left(\bar{I}_p^{a,b,c} - \bar{I}_l^{a,b,c}\right) + \ldots \\
&\quad + \mathbf{Z}_{1q}^{a,b,c}\left(\bar{I}_q^{a,b,c} + \bar{I}_l^{a,b,c}\right) + \ldots + \mathbf{Z}_{1m}^{a,b,c}\bar{I}_m^{a,b,c} \\
&\vdots \\
\bar{V}_p^{a,b,c} &= \mathbf{Z}_{p1}^{a,b,c}\bar{I}_1^{a,b,c} + \ldots + \mathbf{Z}_{pp}^{a,b,c}\left(\bar{I}_p^{a,b,c} - \bar{I}_l^{a,b,c}\right) + \ldots \\
&\quad + \mathbf{Z}_{pq}^{a,b,c}\left(\bar{I}_q^{a,b,c} + \bar{I}_l^{a,b,c}\right) + \ldots + \mathbf{Z}_{pm}^{a,b,c}\bar{I}_m^{a,b,c} \\
&\vdots \\
\bar{V}_q^{a,b,c} &= \mathbf{Z}_{q1}^{a,b,c}\bar{I}_1^{a,b,c} + \ldots + \mathbf{Z}_{qp}^{a,b,c}\left(\bar{I}_p^{a,b,c} - \bar{I}_l^{a,b,c}\right) + \ldots \\
&\quad + \mathbf{Z}_{qq}^{a,b,c}\left(\bar{I}_q^{a,b,c} + \bar{I}_l^{a,b,c}\right) + \ldots + \mathbf{Z}_{qm}^{a,b,c}\bar{I}_m^{a,b,c} \\
&\vdots \\
\bar{V}_m^{a,b,c} &= \mathbf{Z}_{m1}^{a,b,c}\bar{I}_1^{a,b,c} + \ldots + \mathbf{Z}_{mp}^{a,b,c}\left(\bar{I}_p^{a,b,c} - \bar{I}_l^{a,b,c}\right) + \ldots \\
&\quad + \mathbf{Z}_{mq}^{a,b,c}\left(\bar{I}_q^{a,b,c} + \bar{I}_l^{a,b,c}\right) + \ldots \\
&\quad + \mathbf{Z}_{mm}^{a,b,c}\bar{I}_m^{a,b,c}
\end{aligned} \tag{26}$$

Substituting $\bar{V}_p^{a,b,c}$ and $\bar{V}_q^{a,b,c}$ from (26) into (25), yields

$$\begin{aligned}
&\left(\mathbf{Z}_{q1}^{a,b,c} - \mathbf{Z}_{p1}^{a,b,c}\right)\bar{I}_1^{a,b,c} \\
&\quad + \ldots + \left(\mathbf{Z}_{qp}^{a,b,c} - \mathbf{Z}_{pp}^{a,b,c}\right)\bar{I}_p^{a,b,c} + \ldots \\
&\quad + \left(\mathbf{Z}_{qq}^{a,b,c} - \mathbf{Z}_{pq}^{a,b,c}\right)\bar{I}_q^{a,b,c} + \ldots \\
&\quad + \left(\mathbf{Z}_{qm}^{a,b,c} - \mathbf{Z}_{pm}^{a,b,c}\right)\bar{I}_m^{a,b,c} \\
&\quad + \left(\mathbf{z}_{pq}^{a,b,c} + \mathbf{Z}_{pp}^{a,b,c} + \mathbf{Z}_{qq}^{a,b,c} - 2\mathbf{Z}_{pq}^{a,b,c}\right)\bar{I}_l^{a,b,c} = 0
\end{aligned} \tag{27}$$

By adding (27) to (26), the $(m+1)$-th associative equations can be obtained as follows:

$$\begin{bmatrix} \bar{V}_1^{a,b,c} \\ \vdots \\ \bar{V}_p^{a,b,c} \\ \vdots \\ \bar{V}_q^{a,b,c} \\ \vdots \\ \bar{V}_m^{a,b,c} \\ 0 \end{bmatrix} = \left[\begin{array}{ccccccc|c} \mathbf{Z}_{11}^{a,b,c} & \cdots & \mathbf{Z}_{1p}^{a,b,c} & \cdots & \mathbf{Z}_{1q}^{a,b,c} & \cdots & \mathbf{Z}_{1m}^{a,b,c} & \mathbf{Z}_{1l}^{a,b,c} \\ \vdots & \vdots & \vdots & \vdots & \vdots & \vdots & \vdots & \vdots \\ \mathbf{Z}_{p1}^{a,b,c} & \cdots & \mathbf{Z}_{pp}^{a,b,c} & \cdots & \mathbf{Z}_{pq}^{a,b,c} & \cdots & \mathbf{Z}_{pm}^{a,b,c} & \mathbf{Z}_{pl}^{a,b,c} \\ \vdots & \vdots & \vdots & \vdots & \vdots & \vdots & \vdots & \vdots \\ \mathbf{Z}_{q1}^{a,b,c} & \cdots & \mathbf{Z}_{qp}^{a,b,c} & \cdots & \mathbf{Z}_{qq}^{a,b,c} & \cdots & \mathbf{Z}_{qm}^{a,b,c} & \mathbf{Z}_{ql}^{a,b,c} \\ \vdots & \vdots & \vdots & \vdots & \vdots & \vdots & \vdots & \vdots \\ \mathbf{Z}_{m1}^{a,b,c} & \cdots & \mathbf{Z}_{mp}^{a,b,c} & \cdots & \mathbf{Z}_{mq}^{a,b,c} & \cdots & \mathbf{Z}_{mm}^{a,b,c} & \mathbf{Z}_{ml}^{a,b,c} \\ \hline \mathbf{Z}_{l1}^{a,b,c} & \cdots & \mathbf{Z}_{lp}^{a,b,c} & \cdots & \mathbf{Z}_{lq}^{a,b,c} & \cdots & \mathbf{Z}_{lm}^{a,b,c} & \mathbf{Z}_{ll}^{a,b,c} \end{array}\right] \begin{bmatrix} \bar{I}_1^{a,b,c} \\ \vdots \\ \bar{I}_p^{a,b,c} \\ \vdots \\ \bar{I}_q^{a,b,c} \\ \vdots \\ \bar{I}_m^{a,b,c} \\ \bar{I}_l^{a,b,c} \end{bmatrix} \tag{28}$$

where

$$\begin{aligned}
\mathbf{Z}_{li}^{a,b,c} &= \mathbf{Z}_{il}^{a,b,c} \\
&= \mathbf{Z}_{iq}^{a,b,c} - \mathbf{Z}_{ip}^{a,b,c}, \quad i \in \{1,\ldots,p,\ldots,q,\ldots,m\}
\end{aligned} \tag{29}$$

$$\mathbf{Z}_{ll}^{a,b,c} = \mathbf{z}_{pq}^{a,b,c} + \mathbf{Z}_{pp}^{a,b,c} + \mathbf{Z}_{qq}^{a,b,c} - 2\mathbf{Z}_{pq}^{a,b,c} \tag{30}$$

The link currents $\bar{I}_l^{a,b,c}$ can then be eliminated, and (28) can be partitioned and rewritten in a condensed form as follows:

$$\begin{bmatrix} \bar{V}_{BUS}^{a,b,c} \\ 0 \end{bmatrix} = \begin{bmatrix} \mathbf{Z}_{BUS}^{\text{old}} & \Delta\mathbf{Z} \\ \Delta\mathbf{Z}^t & \mathbf{Z}_{ll}^{a,b,c} \end{bmatrix} \begin{bmatrix} \bar{I}_{BUS}^{a,b,c} \\ \bar{I}_l^{a,b,c} \end{bmatrix} \tag{31}$$

where

$$\begin{aligned}
\Delta\mathbf{Z} = \Big[&\mathbf{Z}_{1q}^{a,b,c} - \mathbf{Z}_{1p}^{a,b,c}, \ldots, \mathbf{Z}_{pq}^{a,b,c} \\
&- \mathbf{Z}_{pp}^{a,b,c}, \ldots, \mathbf{Z}_{qq}^{a,b,c} - \mathbf{Z}_{qp}^{a,b,c}, \ldots, \mathbf{Z}_{mq}^{a,b,c} - \mathbf{Z}_{mp}^{a,b,c}\Big]^t
\end{aligned} \tag{32}$$

Therefore, by expanding (31), yields

$$\bar{V}_{BUS}^{a,b,c} = \mathbf{Z}_{BUS}^{\text{old}}\bar{I}_{BUS}^{a,b,c} + \Delta\mathbf{Z}\cdot\bar{I}_l^{a,b,c} \tag{33}$$

$$0 = \Delta\mathbf{Z}^t\bar{I}_{BUS}^{a,b,c} + \mathbf{Z}_{ll}^{a,b,c}\bar{I}_l^{a,b,c} \tag{34}$$

After rearranging (34), yields

$$\bar{I}_l^{a,b,c} = -\left[\mathbf{Z}_{ll}^{a,b,c}\right]^{-1}\Delta\mathbf{Z}^t\bar{I}_{BUS}^{a,b,c} \tag{35}$$

Then, substituting (35) into (33), we have

$$\bar{V}_{BUS}^{a,b,c} = \left[\mathbf{Z}_{BUS}^{\text{old}} - \Delta\mathbf{Z}\cdot\left[\mathbf{Z}_{ll}^{a,b,c}\right]^{-1}\cdot\Delta\mathbf{Z}^t\right]\bar{I}_{BUS}^{a,b,c} \tag{36}$$

Consequently, the new impedance matrix $\mathbf{Z}_{BUS}^{\text{new}}$ is defined by (37).

$$\mathbf{Z}_{BUS}^{\text{new}} = \mathbf{Z}_{BUS}^{\text{old}} - \Delta\mathbf{Z}\cdot\left[\mathbf{Z}_{ll}^{a,b,c}\right]^{-1}\cdot\Delta\mathbf{Z}^t \tag{37}$$

When bus q is the reference, as shown in Fig. 10 (b), then $\mathbf{Z}_{qi}^{a,b,c} = \mathbf{Z}_{iq}^{a,b,c} = 0$, and (28) can be simplified as:

$$\begin{bmatrix} \bar{V}_1^{a,b,c} \\ \vdots \\ \bar{V}_p^{a,b,c} \\ \vdots \\ \bar{V}_m^{a,b,c} \\ \hline 0 \end{bmatrix} = \left[\begin{array}{ccccc|c} \mathbf{Z}_{11}^{a,b,c} & \cdots & \mathbf{Z}_{1p}^{a,b,c} & \cdots & \mathbf{Z}_{1m}^{a,b,c} & -\mathbf{Z}_{1p}^{a,b,c} \\ \vdots & \vdots & \vdots & \vdots & \vdots & \vdots \\ \mathbf{Z}_{p1}^{a,b,c} & \cdots & \mathbf{Z}_{pp}^{a,b,c} & \cdots & \mathbf{Z}_{pm}^{a,b,c} & -\mathbf{Z}_{pp}^{a,b,c} \\ \vdots & \vdots & \vdots & \vdots & \vdots & \vdots \\ \mathbf{Z}_{m1}^{a,b,c} & \cdots & \mathbf{Z}_{mp}^{a,b,c} & \cdots & \mathbf{Z}_{mm}^{a,b,c} & -\mathbf{Z}_{mp}^{a,b,c} \\ \hline -\mathbf{Z}_{p1}^{a,b,c} & \cdots & -\mathbf{Z}_{pp}^{a,b,c} & \cdots & -\mathbf{Z}_{pm}^{a,b,c} & \mathbf{Z}_{ll}^{a,b,c} \end{array}\right] \begin{bmatrix} \bar{I}_1^{a,b,c} \\ \vdots \\ \bar{I}_p^{a,b,c} \\ \vdots \\ \bar{I}_m^{a,b,c} \\ \hline \bar{I}_l^{a,b,c} \end{bmatrix} \tag{38}$$

where $\mathbf{Z}_{ll}^{a,b,c} = \mathbf{z}_{pq}^{a,b,c} + \mathbf{Z}_{pp}^{a,b,c}$ and

$$\Delta\mathbf{Z} = \left[-\mathbf{Z}_{1p}^{a,b,c}, \ldots, -\mathbf{Z}_{pp}^{a,b,c}, \ldots - \mathbf{Z}_{mp}^{a,b,c}\right]^t.$$

IV. PROPOSED ALGORITHM

In this study, the three-phase direct $\mathbf{Z}_{BUS}$ power flow method is improved for unbalanced radial distribution systems by combining the graph theory, Kron reduction method, and superposition theorem. Convergent problems caused by distribution transformers are considered in the proposed method.

In the existing direct $\mathbf{Z}_{BUS}$ power flow method, the slack bus is generally regarded as an ideal voltage source, and the series impedances of the network components are incorporated into the bus impedance matrix according to (23). The shunt components are equivalent to the injection currents, which are updated according to the calculated bus voltages during the iterative process. When all bus voltage mismatches are less than the preset tolerance ε, the bus voltages converge.

However, the direct $\mathbf{Z}_{BUS}$ method may require a large number of iterations or even fail to converge owing to differences in the network component models. Therefore, a bus impedance matrix $\mathbf{Z}_{BUS}$ building algorithm for the series and shunt network components is used in the proposed algorithm. Using equation (23), the series components are incorporated into the bus impedance matrix $\mathbf{Z}_{BUS}$, and using (37), the shunt components are involved in the bus impedance matrix $\mathbf{Z}_{BUS}$. To describe the proposed method, a radial distribution system with series and shunt components is illustrated in Fig. 11.

The proposed direct power flow method is based on bus voltage calculation. Using the superposition theorem, only one type of power source is considered simultaneously when calculating the bus voltage. When a voltage source for the slack bus acts, all injected currents are open-circuit; conversely, when the injected current sources act, the voltage source for the slack bus is short-circuited.

In general, the power flow calculation designates one of the buses connected to the generators as a slack bus. In a power flow study, the voltage at the slack bus is typically assumed to be in a balanced three-phase state. The amplitude $|V_{slack}|$ and power angle θ_0 for the three phases are given by (39).

$$\bar{V}_{slack}^{a,b,c} = \begin{bmatrix} V_{slack}^a \\ V_{slack}^b \\ V_{slack}^c \end{bmatrix} = \begin{bmatrix} |V_{slack}|\angle\theta_0 + 0^\circ \\ |V_{slack}|\angle\theta_0 - 120^\circ \\ |V_{slack}|\angle\theta_0 + 120^\circ \end{bmatrix} \tag{39}$$

Because the ground of the slack bus is considered, according to Norton's theorem, the open-circuit voltage source can be converted into an injection current source with equivalent impedance or admittance. Thus, the equivalent injection current at the slack bus is calculated using (40).

$$\bar{I}_{slack}^{a,b,c} = \left[Z_{BUS,slack}^{a,b,c}\right]_{3\times3}^{-1} \cdot \bar{V}_{slack}^{a,b,c} \tag{40}$$

When the voltage source at the slack bus acts, all the injected current sources are open-circuit. The voltage drops caused by the voltage source at the slack bus are given by (41).

$$\bar{V}_{BUS}^{slack} = \mathbf{Z}_{BUS}^{a,b,c}\bar{I}_{BUS}^{a,b,c} = \begin{bmatrix} \bar{V}_{slack}^{a,b,c} \\ \bar{V}_2^{a,b,c} \\ \bar{V}_3^{c} \\ \bar{V}_4^{a,b,c} \\ \bar{V}_5^{a,b} \\ \bar{V}_6^{a} \end{bmatrix} = \left[\begin{array}{c|ccccc} \mathbf{Z}_{BUS,slack}^{a,b,c} & \mathbf{Z}_{12} & \mathbf{Z}_{13} & \mathbf{Z}_{14} & \mathbf{Z}_{15} & \mathbf{Z}_{16} \\ \hline \mathbf{Z}_{21} & \mathbf{Z}_{22} & \mathbf{Z}_{23} & \mathbf{Z}_{24} & \mathbf{Z}_{25} & \mathbf{Z}_{26} \\ \mathbf{Z}_{31} & \mathbf{Z}_{32} & \mathbf{Z}_{33} & \mathbf{Z}_{34} & \mathbf{Z}_{35} & \mathbf{Z}_{36} \\ \mathbf{Z}_{41} & \mathbf{Z}_{42} & \mathbf{Z}_{43} & \mathbf{Z}_{44} & \mathbf{Z}_{45} & \mathbf{Z}_{46} \\ \mathbf{Z}_{51} & \mathbf{Z}_{52} & \mathbf{Z}_{53} & \mathbf{Z}_{54} & \mathbf{Z}_{55} & \mathbf{Z}_{56} \\ \mathbf{Z}_{61} & \mathbf{Z}_{62} & \mathbf{Z}_{63} & \mathbf{Z}_{64} & \mathbf{Z}_{65} & \mathbf{Z}_{66} \end{array}\right] \begin{bmatrix} \bar{I}_{slack}^{a,b,c} \\ 0 \\ 0 \\ 0 \\ 0 \\ 0 \end{bmatrix} \tag{41}$$

If the network components in the distribution systems have constant or quasi-constant impedance characteristics, the voltage drops calculated by (41) are the final converged solutions without the iterative process. If the distribution system contains network components with constant current or constant power characteristics, the injected current compensations $\bar{I}_{ZIP}^{a,b,c}$ are used to update the voltage drops using (8) during the iterative process. In contrast to (41), when compensating currents are applied, the bus impedance matrix $\mathbf{Z}_{BUS}^{com}$ is used. $\mathbf{Z}_{BUS}^{com}$ is obtained by short-circuiting the slack bus using (37). In the k-th iteration, the voltage drop $\bar{V}_{BUS}^{com}$ caused by the compensating currents can be determined using (42).

$$\bar{V}_{BUS}^{com(k)} = \mathbf{Z}_{BUS}^{com}\bar{I}_{ZIP}^{a,b,c^{(k)}} \tag{42}$$

Therefore, by combining the voltage drops generated by the voltage source at the slack bus and the compensation currents, the bus voltages at the k-th iteration are obtained using (43).

$$\bar{V}_{BUS}^{a,b,c^{(k)}} = \bar{V}_{BUS}^{slack} + \bar{V}_{BUS}^{com(k)} = \bar{V}_{BUS}^{slack} + \mathbf{Z}_{BUS}^{com}\bar{I}_{ZIP}^{a,b,c^{(k)}} \tag{43}$$

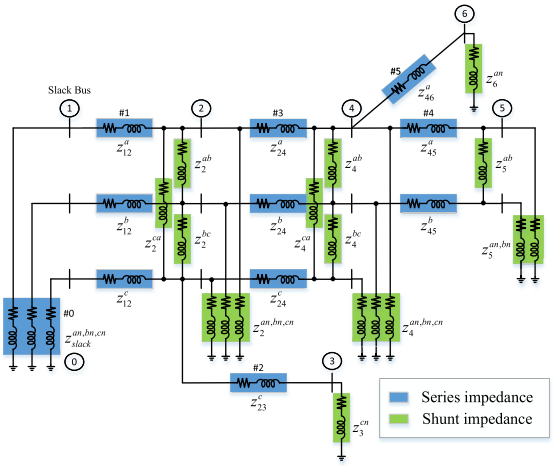

FIGURE 11. Radial distribution system expressed by equivalent impedances.

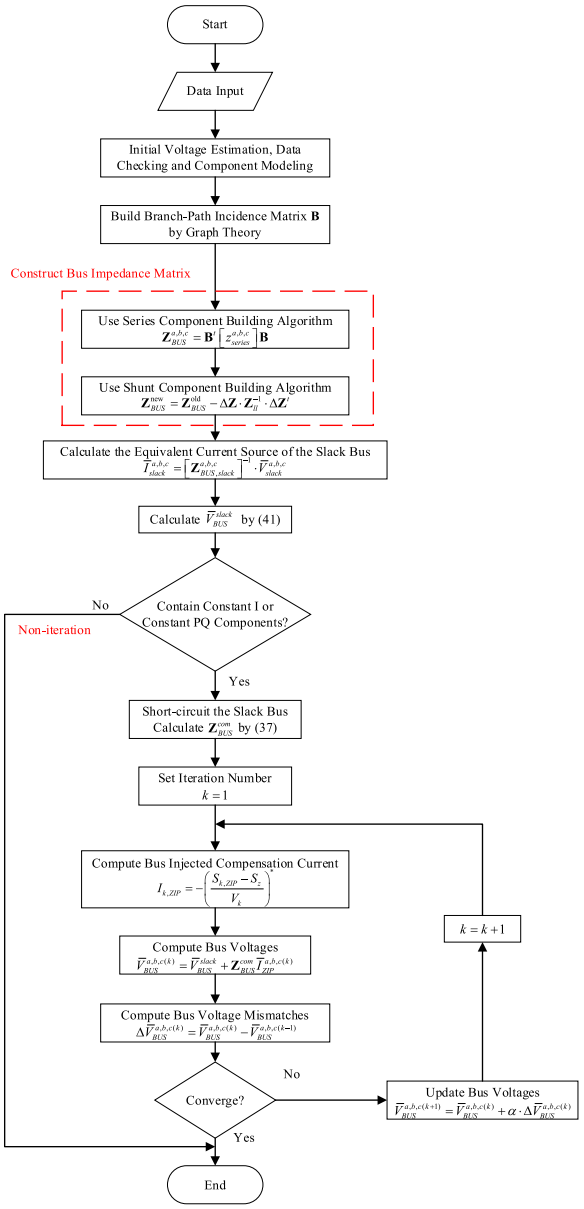

FIGURE 12. Flow chart of the proposed algorithm.

Then, the voltage mismatch at the k-th iteration is

$$\Delta \bar{V}_{BUS}^{a,b,c^{(k)}} = \bar{V}_{BUS}^{a,b,c^{(k)}} - \bar{V}_{BUS}^{a,b,c^{(k-1)}} \tag{44}$$

According to (44), if the voltage mismatches of all buses are less than the predefined tolerance ε, i.e., $\left|\Delta \bar{V}_{BUS}^{a,b,c^{(k)}}\right| < \varepsilon$, then the bus voltages are the final converged solutions; otherwise, the bus voltages are updated iteratively, as shown in (45). A convergence factor α is used to avoid divergence in the power flow calculations during the voltage iteration process, where α is set according to different scenarios for distribution systems, and usually $\alpha \leq 1$. The flowchart of the proposed algorithm is shown in Fig. 12.

$$\bar{V}_{BUS}^{a,b,c^{(k+1)}} = \bar{V}_{BUS}^{a,b,c^{(k)}} + \alpha \cdot \Delta \bar{V}_{BUS}^{a,b,c^{(k)}} \tag{45}$$

V. RESULTS

To confirm the accuracy, robustness, and feasibility of the proposed algorithm, a series of simulations for the accuracy and performance tests were conducted. For all the test cases, the convergence tolerance for the bus voltage was 10^{-4} pu. The program was implemented using MATLAB 2021a on a computer with an i7-10700F processor and Windows 10 operating environment.

A. ACCURACY TEST

In terms of accuracy, the proposed algorithm was compared with the IEEE results. The IEEE-13 bus system contains most of the network components of a practical power grid, including transformers, voltage regulators, shunt capacitor banks, overhead transmission lines, underground cables, and various load demands. Therefore, it is often used as a benchmark for power flow algorithms for unbalanced distribution systems. Table 1 shows the results obtained using the proposed method for power flow calculation. Tables 2 and 3 show the voltage mismatches between the results obtained by the proposed method and IEEE results.

TABLE 1. Bus voltages for IEEE-13 system.

Bus ID	V_{an}	V_{bn}	V_{cn}
650	$1.0000\angle 0.00^\circ$	$1.0000\angle -120.00^\circ$	$1.0000\angle 120.00^\circ$
RG60	$1.0625\angle 0.00^\circ$	$1.0500\angle -120.00^\circ$	$1.0687\angle 120.00^\circ$
632	$1.0210\angle -2.49^\circ$	$1.0420\angle -121.72^\circ$	$1.0175\angle 117.83^\circ$
633	$1.0180\angle -2.55^\circ$	$1.0401\angle -121.77^\circ$	$1.0149\angle 117.83^\circ$
634	$0.9940\angle -3.23^\circ$	$1.0218\angle -122.22^\circ$	$0.9961\angle 117.35^\circ$
645		$1.0328\angle -121.90^\circ$	$1.0155\angle 117.86^\circ$
646		$1.0311\angle -121.98^\circ$	$1.0135\angle 117.90^\circ$
671	$0.9900\angle -5.30^\circ$	$1.0529\angle -122.34^\circ$	$0.9779\angle 116.03^\circ$
680	$0.9900\angle -5.30^\circ$	$1.0529\angle -122.34^\circ$	$0.9779\angle 116.03^\circ$
684	$0.9981\angle -5.32^\circ$		$0.9759\angle 115.93^\circ$
611			$0.9739\angle 115.78^\circ$
652	$0.9825\angle -5.24^\circ$		
692	$0.9900\angle -5.30^\circ$	$1.0529\angle -122.34^\circ$	$0.9779\angle 116.03^\circ$
675	$0.9835\angle -5.55^\circ$	$1.0553\angle -122.52^\circ$	$0.9760\angle 116.04^\circ$

TABLE 2. Magnitude mismatches bus voltages between the calculated solutions and IEEE-13 bus system results.

Bus ID	V_{an}		V_{bn}		V_{cn}	
	p.u.	%	p.u.	%	p.u.	%
650	0.0000	0.0000	0.0000	0.0000	0.0000	0.0000
RG60	0.0000	0.0000	0.0000	0.0000	0.0000	0.0000
632	0.0000	0.0000	0.0000	0.0000	0.0001	-0.0098
633	0.0000	0.0000	0.0000	0.0000	0.0001	-0.0099
634	0.0000	0.0000	0.0000	0.0000	0.0001	-0.0100
645			-0.0001	0.0097	0.0000	0.0000
646			0.0000	0.0000	0.0001	-0.0099
671	0.0000	0.0000	0.0000	0.0000	0.0001	-0.0102
680	0.0000	0.0000	0.0000	0.0000	0.0001	-0.0102
684	0.0000	0.0000			0.0001	-0.0102
611					0.0001	-0.0102
652	0.0000	0.0000				
692	0.0000	0.0000	0.0000	0.0000	0.0002	-0.0205
675	0.0000	0.0000	0.0000	0.0000	0.0002	-0.0205

The results show that the mismatches between the proposed method and the IEEE-13 bus system results are

TABLE 3. Angle mismatches of bus voltages between the calculated solutions and IEEE-13 bus system results.

Bus ID	V_{an}		V_{bn}		V_{cn}	
	degree	%	degree	%	degree	%
650	0.0000	0.0000	0.0000	0.0000	0.0000	0.0000
RG60	0.0000	0.0000	0.0000	0.0000	0.0000	0.0000
632	0.0000	0.0000	0.0000	0.0000	0.0000	0.0000
633	-0.0100	0.3906	0.0000	0.0000	0.0100	-0.0085
634	0.0000	0.0000	0.0000	0.0000	0.0100	-0.0085
645			0.0000	0.0000	0.0000	0.0000
646			0.0000	0.0000	0.0000	0.0000
671	0.0000	0.0000	0.0000	0.0000	0.0100	-0.0086
680	0.0000	0.0000	0.0000	0.0000	0.0100	-0.0086
684	0.0000	0.0000			0.0100	-0.0086
611					0.0000	0.0000
652	0.0100	0.1905				
692	0.0100	0.1883	0.0000	0.0000	0.0100	-0.0086
675	0.0100	0.1799	0.0000	0.0000	0.0100	-0.0086

insignificant. The maximum mismatch of the voltage magnitudes is 0.0002 p.u. (0.0205%), and the maximum mismatch of the voltage angles is 0.01° (0.3906%). There is one reason for this minor mismatch. A different voltage regulator model was used in the proposed algorithm. For the voltage regulator model, three single-phase double-winding transformers were used in this study, whereas the ideal voltage regulator was used in the IEEE test system.

B. PERFORMANCE TEST

To verify the performance of the proposed method, the following tests and analyses were performed in different scenarios using the other five methods.

Method 1— Direct $\mathbf{Z}_{BUS}$ method [12];
Method 2— Implicit Gauss $\mathbf{Z}_{BUS}$ method [25];
Method 3— NR method;
Method 4— CIM method [26];
Method 5— BFS method [10];
Method 6— Proposed method.

1) IEEE TEST CASES

IEEE 13, 34, 37, and 123 bus test systems [27] are often used to verify the convergence of the power-flow algorithm. The selection of network component models and calculation algorithms significantly affects the performance of the solution algorithm. Thus, a performance comparison with existing methods is proposed. TABLE 4 compares the number of iterations (NIs) and execution time (ET) for different test systems. The initial voltage estimation obtained by the proposed method approximates the final converged solution. Hence, the performance of the proposed method is quite excellent than that of the direct $\mathbf{Z}_{BUS}$ and implicit Gauss $\mathbf{Z}_{BUS}$ methods in terms of the NIs, particularly for the IEEE-34 bus system.

Owing to the extensive length of overhead lines and unbalanced loading patterns, the convergence of power flow solution algorithms is challenging. The convergence factor was used during the iterative process.

2) TRANSFORMER CONNECTION TEST CASES

In this subsection, the effects of transformers with different connections on the convergence of solution algorithms are examined. The IEEE-4 bus system [28], as shown in Fig. 13, is often used to test the effects of the transformers. In this test case, the transformer was a step-down transformer with a balanced three-phase load connected to the terminal bus. NI and ET were compared in five connection scenarios for three similar algorithms (Method 1, Method 2, and Method 6). The results are shown in Fig. 14 for the Yg − Yg, Yg − Δ, Y − Δ, Δ − *Yg*, and Δ − Δ connections.

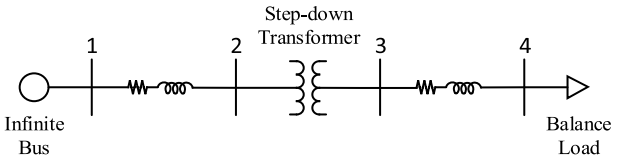

FIGURE 13. IEEE-4 bus system.

In terms of NI, it can be seen that the implicit Gauss $\mathbf{Z}_{BUS}$ method has the worst convergence among the three algorithms. The implicit Gauss $\mathbf{Z}_{BUS}$ method has divergence problems for transformer connections Δ − *Yg* and Δ − Δ. The NIs of the proposed method are reduced by up to 2–6 (28.57%-75%) compared with those of the direct $\mathbf{Z}_{BUS}$ method. The ET of the proposed method is the fastest compared with those of the other algorithms. The proposed method exhibits excellent convergence when considering transformer models.

3) CONSTANT Z LOAD TEST CASE

In the proposed algorithm, if the characteristics of the network components are constant impedance or quasi-constant impedance, then the equivalent compensation currents for the network components are zero. In other words, the network systems consist of only equivalent voltage sources, so the bus voltage can be obtained without an iterative process.

TABLE 4. Comparisons of IEEE test feeder.

Case	Method 1		Method 2		Method 3		Method 4		Method 5		Method 6	
	NI	ET (ms)	NI	ET (ms)	NI	ET (ms)	NI	ET (ms)	NI	ET (ms)	NI	ET (ms)
IEEE-13	4	26.20	4	28.40	4	46.80	5	46.60	5	115.10	3	9.95
IEEE-34	22	393.60	22	391.80	X	X	79	1970.90	85	1935.70	4	68.27
IEEE-37	4	62.60	4	95.40	6	186.30	6	153.70	4	305.60	3	17.73
IEEE-123	10	325.80	10	331.90	73	7548.40	20	1124.60	20	1290.20	4	147.71

* X: The method diverges in this case.

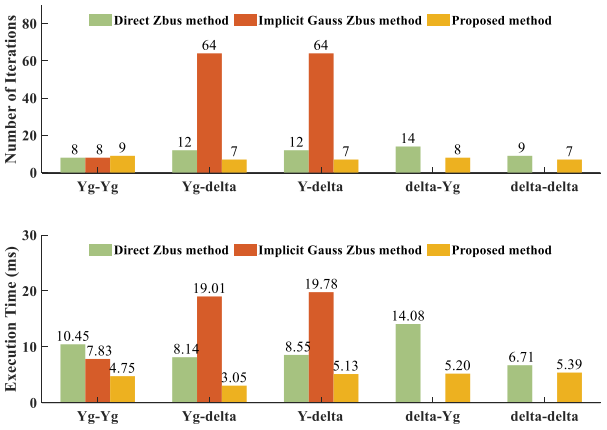

* The implicit Gauss Z_{BUS} method diverges in the case of $\Delta - Yg$ and $\Delta - \Delta$ transformer connections.

FIGURE 14. Comparisons of transformer connections.

TABLE 5. Load parameters for constant Z-13 bus system.

Spot Load Data							
Bus	Load Model	Phase A		Phase B		Phase C	
		P (kW)	Q (kVar)	P (kW)	Q (kVar)	P (kW)	Q (kVar)
634	Y-Z	160	110	120	90	120	90
645	Y-Z			170	125		
646	D-Z			230	132		
652	Y-Z	128	86				
671	D-Z	385	220	385	220	385	220
675	Y-Z	485	190	68	60	290	212
692	D-Z					170	151
611	Y-Z					170	80

Distributed Load Data								
Bus A	Bus B	Load Model	Phase A		Phase B		Phase C	
			P (kW)	Q (kVar)	P (kW)	Q (kVar)	P (kW)	Q (kVar)
632	671	Y-Z	17	10	66	38	117	68

To demonstrate the validity of the proposed direct power flow method, the parameters of the loads in the IEEE-13 bus system were modified, as shown in Table 5. The load characteristics were set to constant impedance. The bus voltages and performance comparisons are presented in Tables 6 and 7.

The proposed algorithm has the advantage of being able to derive bus voltages without iteration when the network components are all constant impedance characteristics. Compared with the other two methods, the proposed method reduces the NIs by 5 (500%) and the ET by 25.95 and 31.15 ms (245.97% and 295.26%).

To demonstrate that the proposed algorithm can be implemented without iterative procedures, two parameters, the load ratio and line ratio were added for a broad range of operating scenarios. The NIs, maximum bus voltage mismatches, and minimum bus voltages were investigated for the constant Z-13 bus system and the IEEE-13 bus system with load ratios and line ratios ranging from 0.6 to 2. The results are presented in Figs. 15–18.

TABLE 6. Bus voltages for constant Z-13 bus system.

Bus ID	V_{an}	V_{bn}	V_{cn}
650	$1.0000\angle 0.00^\circ$	$1.0000\angle -120.00^\circ$	$1.0000\angle 120.00^\circ$
RG60	$1.0625\angle 0.00^\circ$	$1.0500\angle -120.00^\circ$	$1.0687\angle 120.00^\circ$
632	$1.0216\angle -2.36^\circ$	$1.0389\angle -121.84^\circ$	$1.0193\angle 117.82^\circ$
633	$1.0186\angle -2.42^\circ$	$1.0369\angle -121.89^\circ$	$1.0168\angle 117.82^\circ$
634	$0.9949\angle -3.09^\circ$	$1.0178\angle -122.37^\circ$	$0.9981\angle 117.34^\circ$
645		$1.0293\angle -122.03^\circ$	$1.0175\angle 117.85^\circ$
646		$1.0276\angle -122.10^\circ$	$1.0154\angle 117.89^\circ$
671	$0.9909\angle -5.07^\circ$	$1.0481\angle -122.54^\circ$	$0.9810\angle 116.04^\circ$
680	$0.9909\angle -5.07^\circ$	$1.0481\angle -122.54^\circ$	$0.9810\angle 116.04^\circ$
684	$0.9889\angle -5.10^\circ$		$0.9791\angle 115.94^\circ$
611			$0.9772\angle 115.80^\circ$
652	$0.9834\angle -5.02^\circ$		
692	$0.9909\angle -5.07^\circ$	$1.0481\angle -122.54^\circ$	$0.9810\angle 116.04^\circ$
675	$0.9847\angle -5.32^\circ$	$1.0503\angle -122.71^\circ$	$0.9793\angle 116.05^\circ$

TABLE 7. NI and ET for constant Z-13 bus system.

Case	Method 1		Method 2		Method 6	
	NI	ET (ms)	NI	ET (ms)	NI	ET (ms)
13-Bus (Constant Z Load)	6	36.50	6	41.70	1	10.55

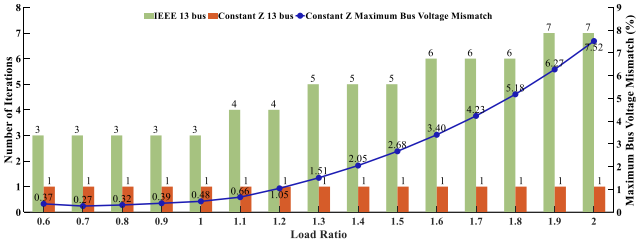

FIGURE 15. Load ratio test case.

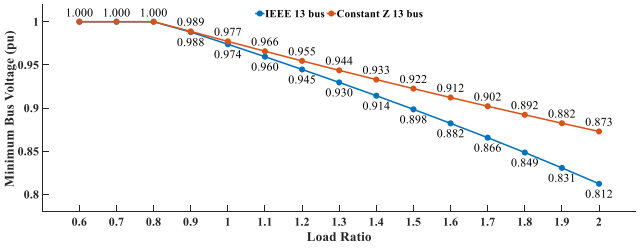

FIGURE 16. Minimum bus voltage in load ratio test case.

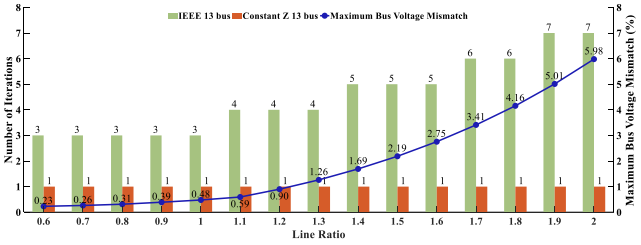

FIGURE 17. Line ratio test case.

The results show that the load and line-length variations may affect the voltage drops in the distribution network, which may affect the NIs. With different load characteristics,

TABLE 8. Test of convergence factor on IEEE test system.

Deceleration factor (α)	Number of iterations											
	IEEE-13 Bus			IEEE-34 Bus			IEEE-37 Bus			IEEE-123 Bus		
	Method 1	Method 2	Method 6	Method 1	Method 2	Method 6	Method 1	Method 2	Method 6	Method 1	Method 2	Method 6
1	4	4	3	X	X	4	4	4	3	20	20	4
0.95	5	5	4	X	X	5	5	5	4	16	16	4
0.9	5	5	4	X	X	5	5	5	4	12	12	5
0.85	6	6	4	X	X	6	6	6	4	13	13	5
0.8	6	6	5	X	X	6	6	6	5	13	13	5
0.75	7	7	5	48	48	7	7	7	5	15	15	6
0.7	8	8	6	24	24	7	7	7	6	16	16	6
0.65	8	8	6	28	28	8	8	8	6	17	17	7
0.6	9	9	7	30	30	9	9	9	7	19	19	8
0.55	10	10	7	33	33	10	10	10	8	21	21	9
0.5	12	12	8	36	36	11	11	11	9	23	23	10
0.45	13	13	9	41	41	13	12	12	10	26	26	11
0.4	15	15	10	46	46	14	14	14	11	30	30	12

X: The method diverges for the case.

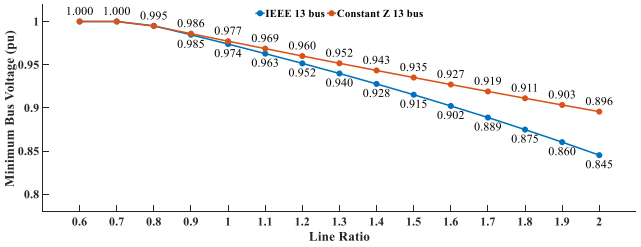

FIGURE 18. Minimum bus voltage in line ratio test case.

increasing the load and line length may slowly increase the NIs. However, with the constant impedance characteristics using the proposed algorithm, the NIs are unaffected. In contrast, the maximum bus voltage mismatch is negligible in the case of a light load or short line length. That is, the minimum bus voltage approaches to 1.0 p.u. The operation conditions can be regarded as the quasi-constant impedance characteristics [29]. Moreover, the initial estimated results for the constant-impedance characteristic can be used instead of the final converged results for the different load characteristics to achieve the bus voltages without the iterative procedure. In conclusion, the comparison results demonstrate the effectiveness of the proposed method.

4) CONVERGENCE FACTOR TEST CASES

To further verify the convergence of the proposed method, the results of the three methods with different convergence factors are compared and analyzed in this subsection. The NIs for the convergence factors from 0.4 to 1 are investigated, as shown in Table 8.

The results show that Methods 1 and 2 require the convergence factor to increase the convergence of the algorithms in the case of complex distribution systems, which is the IEEE-34 bus system. However, the optimal convergence factor varies with the operating conditions of the distribution systems. The optimal convergence factor must be fine-tuned using the trial-and-error method. Nonetheless, the proposed method can improve the convergence of the iterative procedures without considering the convergence factor for all four test systems. Therefore, the proposed method exhibits better convergence than the other two methods.

VI. CONCLUSION

In this study, a three-phase power flow algorithm was proposed for radial distribution networks. The graph theory, Kron reduction method, and superposition theorem were combined in the proposed method. The proposed method involves both the series and shunt components when building the bus impedance matrix. When the network components consist of only a constant impedance characteristic, the bus voltages can be obtained without iterations. If the network component characteristics are constant current or power, only a small amount of compensation current must be injected. Alternatively, the proposed method can achieve a non-iterative procedure in the case of light loads and short lines. To demonstrate the accuracy and efficiency of the proposed method, IEEE test systems were used to verify the convergence performance in terms of the NIs compared to the convergence factor. The proposed method also shows a significant improvement in the NIs and ET compared with the direct $\mathbf{Z}_{BUS}$ method and the implicit Gauss $\mathbf{Z}_{BUS}$ method when transformer models with different connections are considered. Finally, the results demonstrate that the proposed method achieves excellent convergence in unbalanced network systems.

REFERENCES

[1] W. F. Tinney and C. E. Hart, "Power flow solution by Newton's method," *IEEE Trans. Power App. Syst.*, vol. PAS-86, no. 11, pp. 1449–1460, Nov. 1967.
[2] B. Stott and O. Alsac, "Fast decoupled load flow," *IEEE Trans. Power App. Syst.*, vol. PAS-93, no. 3, pp. 859–869, May 1974.
[3] F. Zhang and C. S. Cheng, "A modified Newton method for radial distribution system power flow analysis," *IEEE Trans. Power Syst.*, vol. 12, no. 1, pp. 389–397, Feb. 1997.
[4] S. Iwamoto and Y. Tamura, "A load flow calculation method for ill-conditioned power systems," *IEEE Trans. Power App. Syst.*, vol. PAS-100, no. 4, pp. 1736–1743, Apr. 1981.

[5] D. Rajicic and A. Bose, "A modification to the fast decoupled power flow for networks with high R/X ratios," *IEEE Trans. Power Syst.*, vol. PS-3, no. 2, pp. 743–746, May 1988.

[6] S. C. Tripathy, G. Prasad, O. P. Malik, and G. S. Hope, "Load-flow solutions for ill-conditioned power systems by a Newton-like method," *IEEE Trans. Power App. Syst.*, vol. PAS-101, no. 10, pp. 3648–3657, Oct. 1982.

[7] S. Goswami and S. Basu, "Direct solution of distribution systems," *IEE Proc. C-Gener., Transmiss. Distrib.*, vol. 138, no. 1, pp. 78–88, 1991.

[8] R. G. Cespedes, "New method for the analysis of distribution networks," *IEEE Trans. Power Del.*, vol. 5, no. 1, pp. 391–396, Jan. 1990.

[9] D. Das, H. S. Nagi, and D. P. Kothari, "Novel method for solving radial distribution networks," *IEE Gener., Transmiss. Distrib.*, vol. 141, no. 4, pp. 291–298, Jul. 1994.

[10] W.-M. Lin, Y.-S. Su, J.-H. Teng, and S.-J. Chen, "A new building algorithm for Z-matrix," in *Proc. PowerCon Int. Conf. Power Syst. Technol.*, Dec. 2000, pp. 1041–1046.

[11] D. Sun, S. Abe, R. Shoults, M. Chen, P. Eichenberger, and D. Farris, "Calculation of energy losses in a distribution system," *IEEE Trans. Power App. Syst.*, vol. PAS-99, no. 4, pp. 1347–1356, Jul. 1980.

[12] N. Yang, "Three-phase power flow calculations using direct z BUS method for large-scale unbalanced distribution networks," *IET Gener., Transmiss. Distrib.*, vol. 10, no. 4, pp. 1048–1055, Mar. 2016.

[13] A. Trias, "The holomorphic embedding load flow method," in *Proc. IEEE Power Energy Soc. Gen. Meeting*, Jul. 2012, pp. 1–8.

[14] M. Heidarifar, P. Andrianesis, and M. Caramanis, "Efficient load flow techniques based on holomorphic embedding for distribution networks," in *Proc. IEEE Power Energy Soc. Gen. Meeting (PESGM)*, Aug. 2019, pp. 1–5.

[15] P. S. Sauter, C. A. Braun, M. Kluwe, and S. Hohmann, "Comparison of the holomorphic embedding load flow method with established power flow algorithms and a new hybrid approach," in *Proc. 9th Annu. IEEE Green Technol. Conf. (GreenTech)*, Mar. 2017, pp. 203–210.

[16] M.-S. Chen and T.-H. Chen, "Application of three-phase load flow to power system distribution automation," in *Proc. Int. Conf. Adv. Power Syst. Control, Operation Manage., (APSCOM)*, Nov. 1991, pp. 472–478.

[17] T.-H. Chen, M.-S. Chen, K.-J. Hwang, P. Kotas, and E. A. Chebli, "Distribution system power flow analysis-a rigid approach," *IEEE Trans. Power Del.*, vol. 6, no. 3, pp. 1146–1152, Jul. 1991.

[18] T.-H. Chen, M.-S. Chen, T. Inoue, P. Kotas, and E. A. Chebli, "Three-phase cogenerator and transformer models for distribution system analysis," *IEEE Trans. Power Del.*, vol. 6, no. 4, pp. 1671–1681, Oct. 1991.

[19] W. H. Kersting, *Distribution System Modeling and Analysis*. Boca Raton, FL, USA: CRC Press, 2006.

[20] T.-H. Chen and J.-D. Chang, "Open wye-open delta and open delta-open delta transformer models for rigorous distribution system analysis," *IEE Proc. C Gener., Transmiss. Distrib.*, vol. 139, no. 3, pp. 227–234, 1992.

[21] T.-H. Chen and S.-W. Wang, "Applications of simplified bi-directional feeder models for accelerating the voltage-drop and power-loss calculations," in *Proc. Int. Conf. Energy Manage. Power Del. (EMPD)*, Nov. 1995, pp. 708–713.

[22] D. P. Kothari and I. Nagrath, *Modern Power System Analysis*. New York, NY, USA: McGraw-Hill, 2003.

[23] S. Y. Caliskan and P. Tabuada, "Towards Kron reduction of generalized electrical networks," *Automatica*, vol. 50, no. 10, pp. 2586–2590, 2014.

[24] F. Dörfler and F. Bullo, "Kron reduction of graphs with applications to electrical networks," *IEEE Trans. Circuits Syst. I, Reg. Papers*, vol. 60, no. 1, pp. 150–163, Jan. 2013.

[25] R. D. Zimmerman, *Comprehensive Distribution Power Flow: Modeling, Formulation, Solution Algorithms and Analysis*. New York, NY, USA: Cornell Univ., 1995.

[26] V. M. D. Costa, N. Martins, and J. L. R. Pereira, "Developments in the Newton Raphson power flow formulation based on current injections," *IEEE Trans. Power Syst.*, vol. 14, no. 4, pp. 1320–1326, Nov. 1999.

[27] W. H. Kersting, "Radial distribution test feeders," *IEEE Trans. Power Syst.*, vol. 6, no. 3, pp. 975–985, Aug. 1991.

[28] G. Lammert, D. Premm, and L. D. P. Ospina, "Control of photovoltaic systems for enhanced short-term voltage stability and recovery," *IEEE Trans. Energy Convers.*, vol. 34, no. 1, pp. 243–254, Mar. 2019.

[29] E. R. Ramos, A. G. Exposito, and G. A. Cordero, "Quasi-coupled three-phase radial load flow," *IEEE Trans. Power Syst.*, vol. 19, no. 2, pp. 776–781, May 2004.

NIEN-CHE YANG (Member, IEEE) was born in Keelung, Taiwan, in 1977. He received the B.S., M.S., and Ph.D. degrees in electrical engineering from the National Taiwan University of Science and Technology, Taipei, Taiwan, in 2002, 2004, and 2010, respectively.

Since 2018, he has been a Faculty Member of the National Taiwan University of Science and Technology, where he is currently an Associate Professor in electrical engineering. His research interests include micro-grid state estimation, harmonic three-phase power flow analysis, probabilistic three-phase power flow analysis, energy loss computation in low voltage networks, micro-grids, smart grids, and electric vehicles.

Dr. Yang is a member of the Phi Tau Phi Scholastic Honor Society.

MENG-JIA LIU was born in Taichung, Taiwan, in 1997. He received the B.S. degree from the National Taiwan University of Science and Technology (NTUST), Taipei, Taiwan, in 2020, where he is currently pursuing the M.S. degree with the Electrical Engineering Department.

His research interests include three-phase power flow analysis, passive filter design, micro-grids, and smart grids.

KAI-YOU LAI was born in Miaoli, Taiwan, in 1998. He received the B.S. and M.S. degrees from the National Taiwan University of Science and Technology, Taipei, Taiwan, in 2020 and 2022, respectively.

Currently, he is working at Taiwan Power Company (TPC). His research interests include harmonic three-phase power flow analysis, passive filter design, radial-distribution networks, and smart grids.

EUNIKE WIDYA ADINDA received the B.S. degree from the Institut Teknologi Sepuluh Nopember, Indonesia, in 2019. She is currently pursuing the M.S. degree with the Electrical Engineering Department, National Taiwan University of Science and Technology, Taipei, Taiwan.

Her research interests include harmonic power flow analysis, passive power filter, and radial-distribution networks.